Nanoscale

PAPER

View Article Online
View Journal | View Issue

Cite this: *Nanoscale*, 2017, **9**, 4439

Unique interconnected graphene/SnO_2 nanoparticle spherical multilayers for lithium-ion battery applications†

Qingguo Shao,[a,b] Jie Tang,*[a,b] Yige Sun,[a,b] Jing Li,[a,b] Kun Zhang,[a] Jinshi Yuan,[a] Da-Ming Zhu[c] and Lu-Chang Qin[d]

Received 16th December 2016,
Accepted 29th January 2017

DOI: 10.1039/c6nr09689a

rsc.li/nanoscale

We have designed and synthesized a unique structured graphene/SnO_2 composite, where SnO_2 nanoparticles are inserted in between interconnected graphene sheets which form hollow spherical multilayers. The hollow spherical multilayered structure provides much flexibility to accommodate the configuration and volume changes of SnO_2 in the material. When it is used as an anode material for lithium-ion batteries, such a novel nanostructure can not only provide a stable conductive matrix and suppress the mechanical stress, but also eliminate the need of any binders for constructing electrodes. Electrochemical tests show that the unique graphene/SnO_2 composite electrode as designed could exhibit a large reversible capacity over 1000 mA h g^{-1} and long cycling life with 88% retention after 100 cycles. These results indicate the great potential of the composite for being used as a high performance anode material for lithium-ion batteries.

Introduction

Lithium-ion batteries (LIBs), as the power sources of portable electronic devices and upcoming electric vehicles, have received much attention in recent years.[1–3] The current commercial graphite anode, due to its low theoretical capacity of 372 mA h g^{-1}, cannot meet the demands of future energy storage systems which require both high energy density and power density. Therefore, there has been an urgent need to exploit new high capacity electrode materials to substitute the graphite anode. Transition metal oxides, such as TiO_2, Fe_2O_3, SnO_2, Co_3O_4, MoO_3, NiO, have been studied as the anode materials for LIBs.[4–7] Among them, SnO_2 attracts particular attention because of its large theoretical capacity (782 mA h g^{-1}) and natural abundance.[8–10] However, the SnO_2 anode suffers severe volume expansion (over 200%) during Li^+ insertion and extraction, which could cause the pulverization of the electrodes and loss of interparticle contacts, leading to a low specific capacity and poor cycling stability.[11–17]

Several approaches have been proposed to deal with the problem of the volume changes and to improve the cycling stability of SnO_2 based anodes. One strategy is to decrease the particle size to the nanoscale, which should minimize the strain during the volume expansion.[18] Another strategy involves fabrication of SnO_2 anodes with desired hollow structures, including nanotubes, hollow spheres, and hollow boxes.[19–21] In this strategy, the void space in these hollow structures can accommodate the volume changes and result in enhanced cycling performance. Beside these strategies, making a nanocomposite with a conductive matrix is also useful for buffering the volume expansion as well as improving the electrical conductivity. Among various conductive matrixes, graphene has attracted considerable attention due to its unique properties such as high electrical conductivity, large specific surface area, and broad electrochemical window. Different types of graphene/SnO_2 composites, *e.g.*, graphene mixed SnO_2 composites, graphene loaded SnO_2 composites, graphene wrapped SnO_2 composites, or graphene encapsulated SnO_2 composites, have been fabricated and shown enhanced lithium storage properties.[22–29] However, graphene sheets in those composites tend to form irreversible agglomerates and restack to form graphite due to the strong π–π interactions and van der Waals forces, which could make graphene lose its merits of large surface area and high electrical conductivity and consequently result in rapid capacity fading.[30,31]

[a]*National Institute for Materials Science, 1-2-1 Sengen, Tsukuba 305-0047, Japan. E-mail: tang.jie@nims.go.jp*
[b]*Doctoral Program in Materials Science and Engineering, University of Tsukuba, 1-1-1 Tennodai, Tsukuba 305-8577, Japan. E-mail: tang.jie@nims.go.jp*
[c]*Department of Physics and Astronomy, University of Missouri-Kansas City, Kansas City, MO 64110, USA. E-mail: zhud@umkc.edu*
[d]*Department of Physics and Astronomy, University of North Carolina at Chapel Hill, NC 27599-3255, USA. E-mail: lcqin@unc.edu*

†Electronic supplementary information (ESI) available. See DOI: 10.1039/c6nr09689a

So, it is still a challenge to uniformly load SnO_2 nanoparticles and carefully tailor graphene structures for better electrochemical performances.

In this paper, we report the fabrication of a rationally designed graphene/SnO_2 composite, in which SnO_2 nanoparticles are confined in between multilayered and interconnected graphene spherical sheets. There are several advantages with this design. Firstly, the volume changes of SnO_2 nanoparticles during the charging and discharging process can be restricted by the multi-layered graphene. Secondly, the graphene spheres can serve as a self-separated high conductive substrate to facilitate Li^+ and electron transport. Thirdly, the interconnected nature of graphene hollow spheres makes the electrode self-assemble together, which eliminates the need of binders that could compromise the conductivity and increase the weight of the electrode. Our electrochemical tests show that electrodes with this unique structure of a graphene/SnO_2 composite could exhibit a large reversible capacity over 1000 mA h g^{-1} and excellent long cycling life with 88% retention even after 100 cycles.

Experimental section

The overall synthetic procedure of the proposed graphene/SnO_2 composite is illustrated in Fig. 1. Firstly, an aqueous solution of $SnCl_2{\cdot}2H_2O$ was mixed with graphene oxide (GO) suspension. In this step Sn^{2+} would be hydrolyzed to SnO_2 nanoparticles on both sides of GO to form GO/SnO_2 composite sheets. Then, the pre-synthesized positively charged PS sphere (ESI, Fig. S1†) suspension was added to the above composite sheet mixture. Due to the electrostatic interaction, the composite sheets would wrap around the PS spheres to neutralize the positive charges, resulting in PS@GO/SnO_2 interconnected composite spheres (ESI, Fig. S2†). Finally, the interconnected composite spheres were turned into graphene/SnO_2 composites by heat treatment in which the PS spheres were completely decomposed and GO was thermally reduced to graphene (ESI, Fig. S3†).

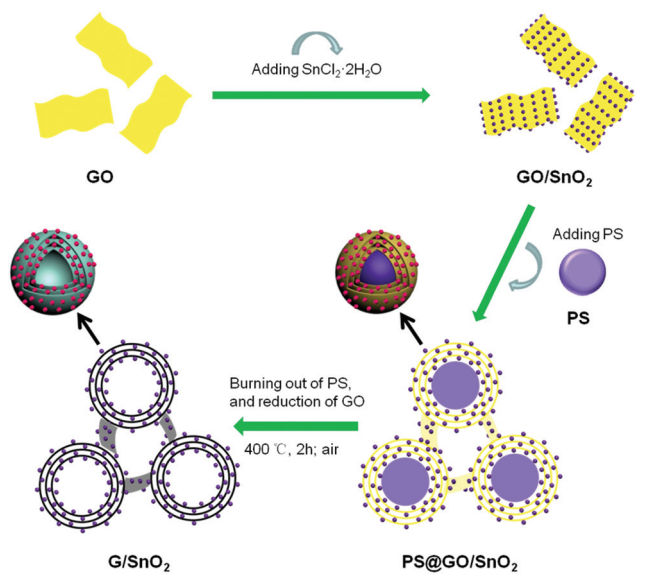

Fig. 1 Illustration of the preparation process of graphene hollow sphere confined SnO_2 nanoparticles.

Synthesis of positively charged polystyrene (PS) spheres

PS spheres were synthesized according to the literature using styrene as a monomer, and AIBA as an initiator. In a typical process, 0.5 g of PVP and 20 mL of styrene were first added to a 250 mL flask containing 100 mL of deionized water. Then, the reaction flask was heated to 70 °C. After stirring for 30 min, 20 mL of deionized water dissolved with 0.2 g of AIBA was added. After reaction for 24 h, the product was centrifuged with deionized water for several times and dried in an oven overnight.

Synthesis of graphene oxide (GO)

Graphene oxide (GO) was synthesized from natural graphite flakes by a modified Hummers method. Briefly, 3.0 g of graphite powder and 1.5 g sodium nitrate were mixed with 70 mL 98 wt% sulfuric acid in an ice-bath. After stirring for 5 min, 9.0 g potassium permanganate was added gradually, and the temperature was kept below 20 °C. The reaction mixture was then transferred to a 35 °C water bath for 1 h, forming a thick paste. Successively, 140 mL of deionized water was slowly added to the pasty mixture. The mixture was stirred for another hour. After being diluted with 500 mL water, the mixture was added slowly with 20 mL of 30% H_2O_2; the color of the mixture changed from dark brown to yellow. The suspension was centrifuged and washed with 10% HCl solution and deionized water several times to remove metal ions and acid. The obtained products were then dried under vacuum until GO powders were formed.

Synthesis of PS@GO/SnO_2 interconnected composite spheres

The synthesis of PS@GO/SnO_2 interconnected composite spheres was conducted as follows: 20 mg of PS was dispersed in 50 mL of deionized water to form solution A. 20 mg of GO, 40 mg of $SnCl_2{\cdot}2H_2O$, and 1 mL of HCl (37% wt%) were dispersed in 50 mL of deionized water to form solution B. Subsequently, the solution B was added to the solution A under vigorous stirring. Then, the mixed solution was kept at 40 °C under stirring for 4 h. Finally, the product was collected by centrifugation and washed with deionized water several times and dried in a vacuum environment.

Synthesis of graphene/SnO_2 composites

The above prepared PS@GO/SnO_2 interconnected composite spheres were calcined at 400 °C in air for 2 h to obtain graphene/SnO_2 composites.

Structural characterization

The morphology and structure of the samples were investigated by field emission scanning electron microscopy (FESEM) (JEOL, JSM-7001F), and transmission electron microscopy (TEM) (JEOL, JEM-2100). X-ray diffraction (XRD) patterns of the samples were

collected on a Rigaku RINT 2500. Raman spectra were recorded with a RAMAN-11 (Nanophoton) with a 532 nm laser source. Thermogravimetric analysis (TGA) was performed on an SDTA851e Analyzer at a heating rate of 10 °C min^{-1} in air. X-ray photoelectron spectroscopy (XPS) data were obtained by a PHI Quantera SXM (Ultravac-PHI). The BET surface area was probed by using an AUTOSORB iQ-MP instrument.

Electrochemical characterization

CR2032 coin-type cells were used to test the electrochemical performance of the samples. Graphene/SnO_2 composites were filtered on a PTFE membrane and cut into circular disks with a diameter of 15 mm. After drying in a vacuum oven at 80 °C for 12 h, the small disks were directly used as the working electrodes. A current collector made of a piece of Cu foil was placed on the sample side of the disks. The test cells were assembled in a glove box, with Li foil as the counter electrode, PP membrane (Celgard 2400) as the separator, and 1 M $LiPF_6$ in a mixture of ethylene (EC) and diethyl carbonate (DEC) (1 : 1, v/v) as the electrolyte. Cyclic voltammograms and galvanostatic charge–discharge measurements were carried out on a VMP3 electrochemical station (Biologic) at voltages between 0.005 V and 2.5 V.

Results and discussion

The morphology of the as prepared graphene/SnO_2 composite was examined using SEM; the representative SEM images in different magnifications are shown in Fig. 2a–c. From the SEM images, we can see that the characteristic sphere like morphology of the composite is retained after spherical particles of PS were decomposed. Also, the self-interconnected feature of the composite spheres is clearly revealed in Fig. 2b and c. Due to this self-interconnected feature, the composite spheres are self-assembled by vacuum filtration on a PTFE paper, as shown in Fig. 2d, and the filtered composite paper can be directly used as an anode for lithium-ion batteries.

The morphology and structure of the as prepared graphene/SnO_2 composite spheres were further characterized using TEM. Fig. 3a shows a typical TEM image of the graphene/SnO_2 composite spheres. As can be seen in the images, SnO_2 nanoparticles are uniformly distributed on the graphene sheets. The spheres are interconnected with a diameter of about 300 nm, which agrees with the SEM results. From the larger TEM image in Fig. 3b, we can clearly see that SnO_2 nanoparticles are confined between the multi-layered graphene sheets and the size of the SnO_2 nanoparticles is about 5 nm. The HR-TEM images in Fig. 3c and the selected area electron diffraction (SEAD) pattern in Fig. 3d confirm the nanoparticles are SnO_2.[11–13,15]

XRD, Raman and TGA techniques were further employed to characterize the chemical structure of the graphene/SnO_2 composite spheres. Fig. 4a shows the XRD pattern of the as prepared composite spheres. The XRD pattern can be well indexed to the tetragonal phase of SnO_2 (JCPDS: 41-1445), which confirms again the existence of SnO_2 in the composite.[18,32–34] It should be noted that the main peak of gra-

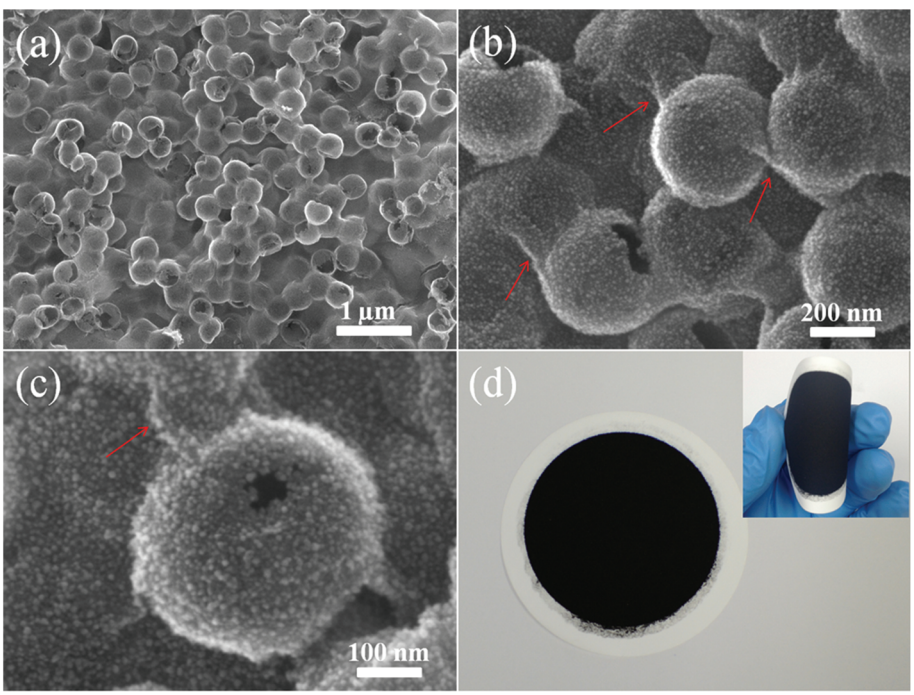

Fig. 2 (a–c) FESEM images of graphene/SnO_2 composites at different magnifications; the arrows highlight the interconnected feature of the composite. (d) A photograph of the graphene/SnO_2 composite filtered on a PTFE membrane showing that it can be self-assembled without any binder. The inset shows its good mechanical flexibility.

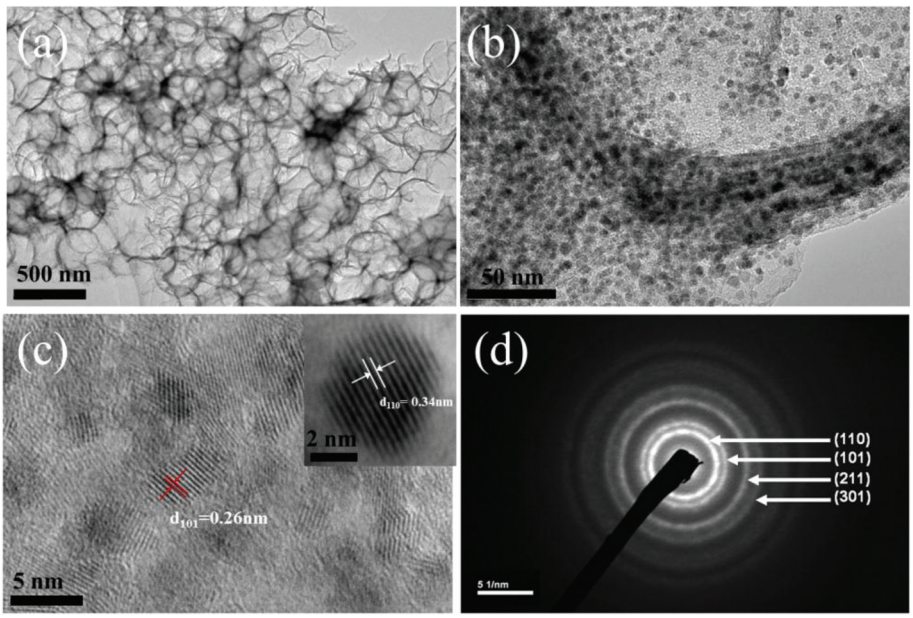

Fig. 3 (a, b) TEM images of graphene/SnO_2 composites at different magnifications; (c) HRTEM images; (d) the selected area electron diffraction (SEAD) pattern of graphene/SnO_2 composites.

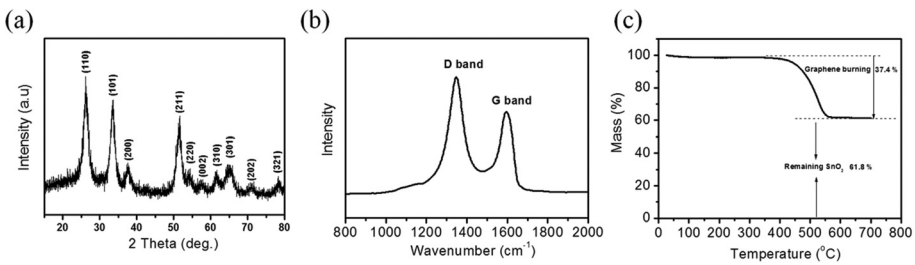

Fig. 4 (a) XRD pattern; (b) Raman spectra; (c) TGA curve of the graphene/SnO_2 composite.

phene (002) is overlapped with the (110) peak of SnO_2, so it is difficult to distinguish the independent diffraction peak of graphene in the XRD pattern. The Raman spectrum shown in Fig. 4b displays the characteristic D band and G band, confirming the formation of graphene during the heating process. Besides, XPS was also performed to further confirm the chemical composition of the spheres (ESI, Fig. S3†). Fig. 4c shows the TGA curve of the as prepared composite spheres which was obtained under ambient conditions. Decomposition of the composite starts at a temperature in the range from 450 to 550 °C, corresponding to the decomposition of graphene in air. The remaining 61.8% weight should only come from SnO_2, and this ratio is consistent with the former TGA results of PS@GO/SnO_2 interconnected composite spheres (ESI, Fig. S4†).

The specific surface area and pore size distribution of an electrode material play a key role in determining the electrochemical performances of the battery. The porosity of the as prepared graphene/SnO_2 composite spheres was investigated using the Brunauer–Emmett–Teller (BET) nitrogen adsorption method performed at 77 K. The BET isotherm measured on the composite sample is shown in Fig. 5. As can be seen in the figure, the measured data form a typical type IV isotherm, indicating a large number of mesopores in the composite. According to the adsorption isotherm, the specific surface area of the composite spheres is 315 $m^2\ g^{-1}$, which is larger than those previously reported for bare SnO_2 and other types of graphene/SnO_2 composites.[35–37] The pore size distribution (shown in the inset) derived from the adsorption isotherm also confirms its large mesopores proportion; the pores are mainly centered in the range of 3–5 nm, which is favorable for the diffusion of Li ions and the electron transfer within the electrode.

We tested the composite spheres as anode materials for lithium ion batteries and the obtained electrochemical performances of the material. Fig. 6a shows the first three CV curves measured on the composite at the scan rate of 0.1 mV s^{-1} and in the potential range of 0.005 to 2.5 V. In the first cycle, the reduction peak of SnO_2 to Sn at 0.7 V corresponds to the formation of a solid electrolyte interface (SEI) layer.[12–14]

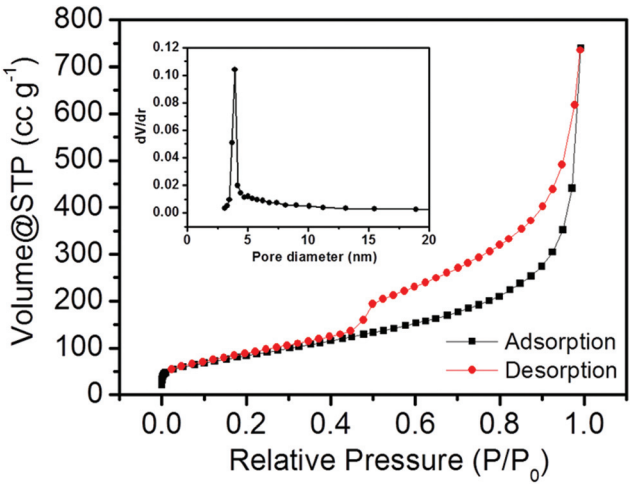

Fig. 5 Nitrogen adsorption–desorption isotherms obtained at 77 K. The inset is the corresponding pore size distribution.

This peak disappears after the first CV cycle, indicating that the SEI layer is stable. There is another sharp reduction peak at 0.1 V, which is assigned to the formation of Li–Sn alloys and the reaction between lithium and graphene sheets. In the anodic curve, two main peaks located at 0.51 and 1.25 V are attributed to the de-alloying of the Li–Sn alloy and the partially reversible reaction of Sn to SnO_2.[12–14] The reversibility of this peak suggests the advantages of this unique structured graphene/SnO_2 composite, such as high electric conductivity, and good contact between SnO_2 and graphene sheets.

Fig. 6b shows the initial three charge–discharge curves of the composite spheres at a current density of 100 mA g^{-1}. In the first discharge curve, the potential plateau at about 0.78 V is associated with the reduction of SnO_2 to Sn. The long flat curve from 0.5 to 0.005 V is the reaction of Sn with Li. The first discharge capacity is 1980 mA h g^{-1}, which is much larger than the first charge capacity of 1032 mA h g^{-1} due to the irreversible formation of Li_2O. This result is in good agreement with the former CV measurement. The reversible capacity in the second discharge process is 1003 mA h g^{-1}, which is among the highest values for SnO_2 based anodes. Fig. 6c displays the cycling performance of the composite spheres. After 100 repeated charge and discharge cycles at a current density of 100 mA g^{-1}; 88% of the initial capacity (883 mA h g^{-1}) is retained and the coulombic efficiency remains nearly 100%, indicating the high cycling stability of the graphene/SnO_2 composite spheres. The TEM images of the composite electrode after 100 cycles (ESI, Fig. S5†) show that the spherical graphene skeleton is preserved and the nanoparticles are well distributed over the sheets without a noticeable change, demonstrating its good structure stability, which reconfirms the crucial role of the interconnected spherical graphene in confining the SnO_2 nanoparticles. The cycling performance is more excellent compared with some previously reported various graphene/SnO_2 composite anodes (ESI, Table S1†). A multiple-step galvanostatic strategy was adopted to test the rate performance of the composite spheres. As shown in Fig. 6d, the reversible discharge capacity is 1003, 778, and 652 mA h g^{-1} at current densities of 100, 200, 500 mA g^{-1}, respectively. Even at a high current density of 1000 mA g^{-1}, the

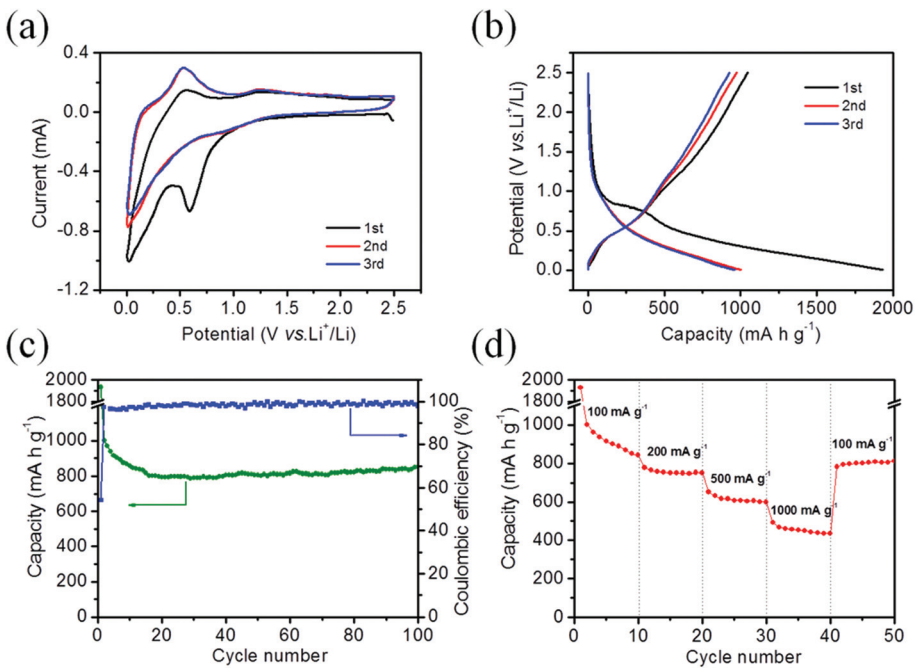

Fig. 6 Electrochemical performance of the graphene/SnO_2 composite. (a) CV curves of the first three cycles at a scan rate of 0.1 mV s^{-1}, (b) charge/discharge curves, (c) cycling stability and coulombic efficiency at 100 mA g^{-1}; (d) rate capability.

composite spheres still exhibit a high specific capacity of 492 mA h g^{-1}, which is much larger than the theoretical capacity of graphite (372 mA h g^{-1}). Besides, when the current density goes back to 100 mA g^{-1}, a high specific capacity of 781 mA h g^{-1} is recovered.

Conclusions

In summary, we report the synthesis and the study of a unique structured graphene/SnO_2 composite where the SnO_2 nanoparticles are confined between the multi-layered sheets of interconnected graphene hollow spheres. The as prepared interconnected composite spheres can self-assemble to form a free standing paper without the use of any binder, allowing the composite to be directly used as an anode material for Li-ion batteries. Electrochemical measurements demonstrate high specific capacity, good rate capability and excellent long cycling performance for the composite. These results indicate the great potential of the composite for being used to construct high performance Li-ion batteries.

Acknowledgements

This work was supported by the JST ALCA Program (no. 22310074), and the NIMS microstructural characterization platform as a program of "Nanotechnology Platform" of the Ministry of Education, Culture, Sports, Science and Technology (MEXT), Japan. This study was also supported by the Shandong Taishan Scholar Program and a fellowship from Japan Society for the Promotion of Science (JSPS).

References

1 A. L. Mohana Reddy, S. R. Gowda, M. M. Shaijumon and P. M. Ajayan, *Adv. Mater.*, 2012, **24**, 5045–5064.
2 Z.-S. Wu, G. Zhou, L.-C. Yin, W. Ren, F. Li and H.-M. Cheng, *Nano Energy*, 2012, **1**, 107–131.
3 B. Luo, S. Liu and L. Zhi, *Small*, 2012, **8**, 630–646.
4 X. Yu, S. Liu and J. Yu, *Appl. Catal., B*, 2011, **104**, 12–20.
5 L.-Y. Hao, C.-L. Zhu, W.-Q. Jiang, C.-N. Chen, Y. Hu and Z.-Y. Chen, *J. Mater. Chem.*, 2004, **14**, 2929.
6 H. Wang, Y. Liang, M. Gong, Y. Li, W. Chang, T. Mefford, J. Zhou, J. Wang, T. Regier, F. Wei and H. Dai, *Nat. Commun.*, 2012, **3**, 917.
7 H. Zhang, X. Yu and P. V. Braun, *Nat. Nanotechnol.*, 2011, **6**, 277–281.
8 S. Yang, W. Yue, J. Zhu, Y. Ren and X. Yang, *Adv. Funct. Mater.*, 2013, **23**, 3570–3576.
9 X. Wang, X. Zhou, K. Yao, J. Zhang and Z. Liu, *Carbon*, 2011, **49**, 133–139.
10 J. S. Chen and X. W. Lou, *Small*, 2013, **9**, 1877–1893.
11 B. Zhang, Q. B. Zheng, Z. D. Huang, S. W. Oh and J. K. Kim, *Carbon*, 2011, **49**, 4524–4534.
12 S. Ding, D. Luan, F. Y. Boey, J. S. Chen and X. W. Lou, *Chem. Commun.*, 2011, **47**, 7155–7157.
13 X. Huang, X. Zhou, L. Zhou, K. Qian, Y. Wang, Z. Liu and C. Yu, *ChemPhysChem*, 2011, **12**, 278–281.
14 J. Yao, X. Shen, B. Wang, H. Liu and G. Wang, *Electrochem. Commun.*, 2009, **11**, 1849–1852.
15 P. Lian, X. Zhu, S. Liang, Z. Li, W. Yang and H. Wang, *Electrochim. Acta*, 2011, **56**, 4532–4539.
16 X. S. Zhou, L. Yu and X. W. Lou, *Nanoscale*, 2016, **8**, 8384–8389.
17 Q.-G. Shao, W.-M. Chen, Z.-H. Wang, L. Qie, L.-X. Yuan, W.-X. Zhang, X.-L. Hu and Y.-H. Huang, *Electrochem. Commun.*, 2011, **13**, 1431–1434.
18 Y. Chen, B. Song, R. M. Chen, L. Lu and J. Xue, *J. Mater. Chem. A*, 2014, **2**, 5688.
19 Y. J. Hong, J. W. Yoon, J. H. Lee and Y. C. Kang, *Chem. – Eur. J.*, 2015, **21**, 371–376.
20 J. Zhang, H. Ren, J. Wang, J. Qi, R. Yu, D. Wang and Y. Liu, *J. Mater. Chem. A*, 2016, **4**, 17673–17677.
21 X. Zhou, L. Yu and X. W. D. Lou, *Adv. Energy Mater.*, 2016, **6**, 1600451.
22 B. P. Vinayan and S. Ramaprabhu, *J. Mater. Chem. A*, 2013, **1**, 3865.
23 Y. Zou, X. Zhou, J. Xie, Q. Liao, B. Huang and J. Yang, *J. Mater. Chem. A*, 2014, **2**, 4524.
24 H. Zhang, P. Xu, Y. Ni, H. Geng, G. Zheng, B. Dong and Z. Jiao, *J. Mater. Res.*, 2014, **29**, 617–624.
25 Z. Du, X. Yin, M. Zhang, Q. Hao, Y. Wang and T. Wang, *Mater. Lett.*, 2010, **64**, 2076–2079.
26 H. Kim, S.-W. Kim, Y.-U. Park, H. Gwon, D.-H. Seo, Y. Kim and K. Kang, *Nano Res.*, 2010, **3**, 813–821.
27 Z. Wang, H. Zhang, N. Li, Z. Shi, Z. Gu and G. Cao, *Nano Res.*, 2010, **3**, 748–756.
28 G. Zhou, D. W. Wang, L. Li, N. Li, F. Li and H. M. Cheng, *Nanoscale*, 2013, **5**, 1576–1582.
29 X. Liu, J. Chen, W. Li, X. Zhong, Z. Yang, L. Gu and Y. Yu, *Nanoscale*, 2014, **6**, 7817.
30 Q. Shao, J. Tang, Y. Lin, J. Li, F. Qin, J. Yuan and L.-C. Qin, *J. Power Sources*, 2015, **278**, 751–759.
31 Q. Shao, J. Tang, Y. Lin, J. Li, F. Qin, K. Zhang, J. Yuan and L.-C. Qin, *Electrochim. Acta*, 2015, **176**, 1441–1446.
32 H. Song, L. Zhang, C. He, Y. Qu, Y. Tian and Y. Lv, *J. Mater. Chem.*, 2011, **21**, 5972.
33 G. Wang, B. Wang, X. Wang, J. Park, S. Dou, H. Ahn and K. Kim, *J. Mater. Chem.*, 2009, **19**, 8378.
34 M. Zhang, D. Lei, Z. Du, X. Yin, L. Chen, Q. Li, Y. Wang and T. Wang, *J. Mater. Chem.*, 2011, **21**, 1673.
35 Y. Wang, Y. Liu and J. Zhang, *J. Nanopart. Res.*, 2015, **17**, 420.
36 R. Tian, Y. Zhang, Z. Chen, H. Duan, B. Xu, Y. Guo, H. Kang, H. Li and H. Liu, *Sci. Rep.*, 2016, **6**, 19195.
37 B. Huang, X. Li, Y. Pei, S. Li, X. Cao, R. Massé and G. Cao, *Small*, 2016, **12**, 1945.

